Available online at www.sciencedirect.com
SCIENCE DIRECT®
ELSEVIER
Journal of Crystal Growth 247 (2003) 371–380
JOURNAL OF CRYSTAL GROWTH
www.elsevier.com/locate/jcrysgro

HRTEM and GIXRD studies of CdS nanocrystals embedded in Al_2O_3 films produced by magnetron RF-sputtering

O. Conde[a], A.G. Rolo[b,*], M.J.M. Gomes[b], C. Ricolleau[c], D.J. Barber[d,1]

[a] *Departamento de Física, Universidade de Lisboa, Campo Grande, Ed. C8, 1749-016 Lisboa, Portugal*
[b] *Departmento de Física, Universidade do Minho, Largo do Paco, Campus de Gualtar, 4710-057 Braga, Portugal*
[c] *Laboratoire de Minéralogie et Cristallographie, Univ. Paris VI et VII, 75252 Paris Cedex 05, France*
[d] *Advanced Materials Group, S.I.M.S., Cranfield University, Cranfield MK43 0AL, UK*

Received 11 June 2002; accepted 24 September 2002
Communicated by T.F. Kuech

Abstract

In this paper we report on the structural properties of as-grown CdS nanoparticles embedded in Al_2O_3 films produced by a magnetron RF-sputtering technique. Grazing incidence X-ray diffraction together with high-resolution transmission electron microscopy (HRTEM) and electron diffraction were used to study the crystallinity and morphology of the CdS nanocrystals. Depending on the deposition parameters, elongated or spherical nanocrystals were grown. HRTEM shows evidence of the growth of CdS nanocrystals at room temperature with sizes in the range of 3–8 nm, and indicates that the nanocrystals formed in the cubic phase during the early stages of the deposition process. Stress-free films were formed under selected deposition conditions.

PACS: 61.10.−i; 61.46.+w; 81.07.Ta; 81.15.Cd

Keywords: A1. Glancing incidence X-ray diffraction; A1. High resolution transmission electron microscopy; A1. RF-sputtering; B1. Nanomaterials; B2. Semiconducting II–VI materials

1. Introduction

The confinement of electrons and phonons are made possible by II–VI semiconductor nanocrystals, when the particle size is of the order of magnitude of the Bohr radius of the exciton, leading to new physical properties. From the technological point of view, these materials have a great potential, for instance in the field of information processing and transmission. However, for both fundamental and technological purposes, it is necessary to control the processing of the materials to achieve the following well-defined structural properties: crystal phase, small particle average size and narrow size distribution.

Nanocrystals of CdS dispersed in dielectric matrices have been produced using several techniques such as melting [1], sol–gel [2],

*Corresponding author. Tel.: +351-253-604065; fax: +351-253-678981.
E-mail address: arolo@fisica.uminho.pt (A.G. Rolo).
[1] Present address: Physics Centre, University of Essex, Colchester CO4 3SQ, UK.

0022-0248/03/$ - see front matter
PII: S0022-0248(02)01975-9

Langmuir–Blodgett [3], colloidal solution [4], deposition from the vapour phase [5], ion-implantation [6] and, more recently, in nanoporous anodised alumina films [7]. Usually the as-prepared films are amorphous at room temperature and the formation and growth of the CdS nanocrystals is induced by post-annealing for various temperatures and times. The size of the nanocrystals is controlled by the annealing conditions and this procedure normally requires high temperatures and several hours of operation, leading to a broad distribution of nanocrystal sizes inside the matrix [1–3,5,6,8]. For anodised alumina films, the nanocrystal size is imposed by the pore dimension, typically 10 nm, and for films produced by ion-beam synthesis the nanocrystals are above 20 nm, i.e. well-above Bohr exciton radius in both cases. By using the RF-sputtering technique at room temperature and by adjusting the deposition parameters, it is possible to control the size of the nanocrystals and the film microstructure, as will be shown below.

Compared to the extensive optical investigations dedicated to semiconductor nanocrystals, there have been few detailed structural studies in these systems [9,10]. The main purpose of this paper is to describe the structural properties (type of phase, particle size and shape) of CdS nanoparticles embedded in Al_2O_3 matrices, grown as micron-thick-films or very thin films (some tens of nanometres) on glass substrates or carbon films, respectively.

2. Experimental procedure

2.1. Sample growth

Alumina and CdS-doped alumina films were produced by conventional RF-magnetron co-sputtering method using an Alcatel SCM 650 apparatus. Al_2O_3 plates (purity of 99.99%), 50 mm diameter, were used as targets. Chips of polycrystalline CdS were placed on top of the alumina plates to make the doped films. Prior to sputtering, the chamber was evacuated to 5×10^{-6} mbar and in situ Ar (99.996%) plasma treatment of targets and substrates was performed in order to clean and remove any surface contaminants. The sputtering was also carried out in an argon atmosphere. The target-substrate distance was kept constant at 55 mm. Samples were deposited on glass slides, Corning glass and (1 1 1) silicon wafers, and a few were deposited on thin amorphous carbon films supported by Cu-grids, especially for HRTEM measurements. The CdS-doped alumina films were produced at different temperatures (from room temperature to 300°C), Ar^+ pressure (1×10^{-3}–10×10^{-3} mbar) and RF-power (30 up to 200 W). Different amounts of CdS on top of the alumina plates were used. The experimental parameters used to produce the Al_2O_3 and CdS/Al_2O_3 films are presented in Table 1. Only samples deposited at room temperature (RT) are discussed in this work.

Table 1
Experimental growth parameters of Al_2O_3 and Al_2O_3+CdS RF-sputtered films

	Al_2O_3	Al_2O_3+CdS
P_{Ar} ($\times 10^{-3}$ mbar)	1–10	1–9
RF–power (W)	50–200	30–200
Substrate temperature (°C)	RT	RT
% of target area covered by CdS	—	4–15
Annealing temperature and time	—	450°C, 2–16 h
Dep. rate (nm/min)	0.9–4.5	0.3–4.0

Some of the as-deposited films were annealed in a furnace filled with argon, at ambient pressure and 450°C, for different annealing times (Table 1).

2.2. Sample characterisation

The thicknesses of the Al_2O_3 and CdS/Al_2O_3 films were determined from optical transmission measurements using the Swanepoel's method [11]. The deposition rates are presented in Table 1, together with the growth conditions.

Structural analysis of the films was carried out in a Siemens D5000 diffractometer by glancing incidence X-ray diffraction (GIXRD), using Cu K_α radiation at 1° angle of incidence to the specimen surface. The identification of crystalline

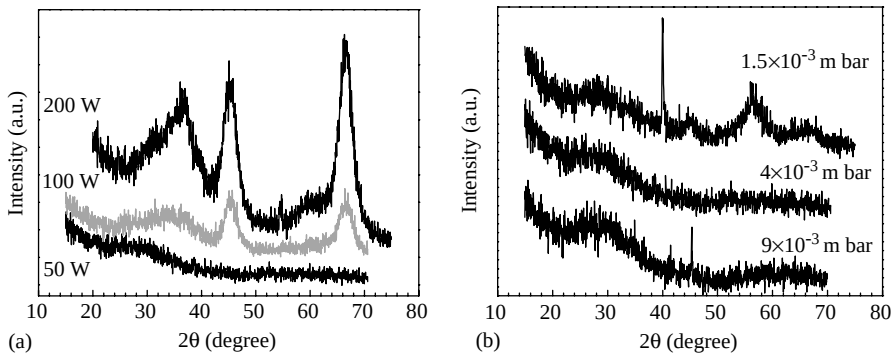

Fig. 1. GIXRD patterns of alumina samples grown under different conditions, as indicated in the graphs, (a) argon pressure = 4×10^{-3} mbar, (b) RF-power = 50 W.

phases was done using the JCPDS database cards.[2,3]

High-resolution transmission electron microscopy (HRTEM) and electron diffraction (ED) studies were conducted in two microscopes: (i) a JEOL 2010 electron microscope equipped with a LaB_6 electron gun operating at 200 kV, with a point to point resolution of 0.19 nm; (ii) a Philips CM20 electron microscope operating at 200 kV with a point to point resolution of 0.27 nm. Two different preparation techniques were used for the samples devoted to TEM analysis. In the most commonly used method, samples were glued, cut at about $3 \times 3\,mm^2$ size and submitted to mechanical thinning down to a few microns thickness, and finally ion milling was applied. The thinned samples were coated with an amorphous carbon layer to avoid charging effects. In the second method, very thin CdS/Al_2O_3 films were grown on top of an amorphous carbon film supported by a copper grid; these samples did not need any further preparation for HRTEM observation and they were placed directly under the electron beam in the microscope. Using this latter technique for sample growth, without extra preparation, we hoped to avoid artifacts. Samples were observed in cross-section and plan-view, and by both bright-field and dark-field imaging. Images were acquired for short periods of time in order to avoid the possibility of diffusion and growth of the crystallites. ED data were also acquired.

3. Results

3.1. Alumina films

The GIXRD patterns of as-grown alumina films are depicted in Fig. 1 and they show a clear dependence on the deposition parameters. The observed changes in Fig. 1a are only due to RF-power: the films deposited at 50 W are amorphous, while those deposited at higher RF-power (100 and 200 W) show already a certain degree of crystallinity. The influence of argon pressure (1.5×10^{-3}, 4×10^{-3} and 9×10^{-3} mbar) for a constant RF-power of 50 W is shown in Fig. 1b.

The refractive index of the alumina films, measured by ellipsometry at 633 nm, varies between 1.6 and 1.7, staying close to the value for alumina films grown by physical vapour deposition (PVD) [12].

3.2. CdS-doped alumina films

The X-ray diffractograms of the CdS-doped alumina films show evidence of three types of samples that can be produced by varying the deposition parameters in the RF-sputtering technique. Spectrum (a) in Fig. 2 is typical of samples produced at low argon pressure, below or equal to

[2] JCPDS cards 16-0394 for Al_2O_3.
[3] JCPDS cards 41-1049 for CdS.

4×10^{-3} mbar, and RF-power values between 30 and 100 W. It consists mainly of a narrow peak centred at about 26° and a broad and low-intensity reflection peak centred at about 47°. These samples will be designated as type 1 samples in what follows.

Keeping the argon pressure at the same low values as above and increasing the RF-power to 200 W, or increasing the argon pressure to 9×10^{-3} mbar and using any of the RF-power values, leads to a dramatic change of the XRD pattern (Fig. 2c). This consists of a large number of reflections, forming a pattern similar to that from a film containing randomly oriented nanocrystallites (type 2 samples).

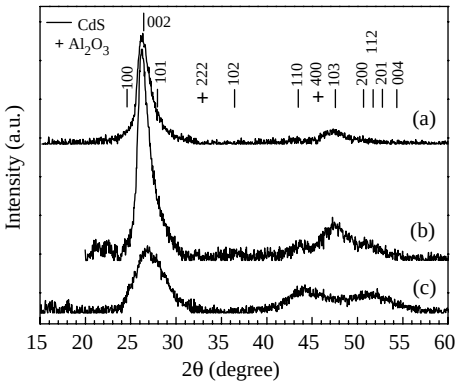

Fig. 2. GIXRD spectra of CdS-doped alumina thin films deposited with the following parameters: (a) 50 W, 4×10^{-3} mbar, (b) 50 W, 9×10^{-3} mbar, (c) 100 W, 9×10^{-3} mbar. Labelled peaks refer to JCPDS cards 41-1049 for CdS and 16-0394 for Al_2O_3.

An intermediate type of sample can be produced for specific deposition parameters, i.e. at high argon pressure but with shorter deposition times than those used for preparation of type 2 samples. The XRD patterns from a typical intermediate sample (Fig. 2b) displays a narrow reflection peak centred at about 26° and a broader one at about 47° as with type 1 samples, but two small broad peaks at about 43° and 51° also start to develop. Therefore, the overall aspect of the diffractogram in the high 2θ region seems to indicate a transition between types 1 and 2 samples.

It is well known from literature that post-annealing treatments promote crystallisation and growth of the nanocrystallites and improve the general quality of thin films deposited by PVD methods [12]. In order to investigate the structural stability of CdS/Al_2O_3 samples, some specimens were annealed at 450°C, in an argon atmosphere, for different annealing times ranging from 2 to 16 h. Fig. 3a shows the GIXRD spectra of a CdS-doped alumina type 1 film, as-deposited (lower curve) and after successive annealing treatments, on the same film (upper curves). Fig. 3b illustrates

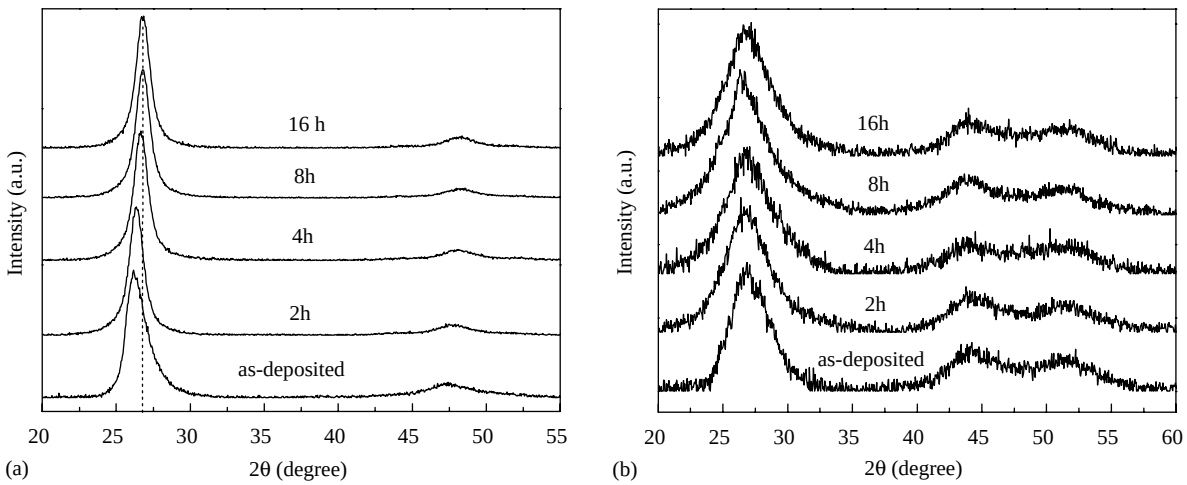

Fig. 3. GIXRD spectra of CdS-doped alumina films, as-deposited and after successive annealing at 450°C, (a) type 1 films—the dashed line highlights the shift of the (0 0 2) peak position as annealing time increases, (b) type 2 films.

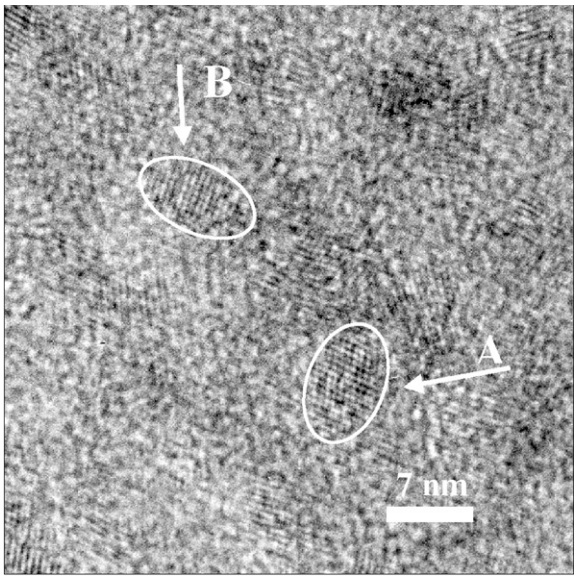

Fig. 4. HRTEM micrograph of a CdS-doped alumina film (~16 nm thick) as-deposited on a carbon-grid, containing particles with a length of ~7.5 nm (indicated by arrows).

diffraction patterns from one type 2 sample, in the as-deposited condition and also when annealed for different total times.

Figs. 4 and 5 show HRTEM micrographs of three different CdS-doped alumina films. In all samples that we examined, the micrographs clearly show the presence of CdS nanocrystals dispersed in an amorphous phase composed of the alumina matrix. The CdS nanocrystals are made evident by the presence of regular sets of lattice fringes corresponding to interplanar spacings that are characteristic of CdS crystallites. TEM images are projections, so that contributions from the surrounding alumina and the amorphous carbon film or carbon coating are superposed on the crystallites and, in the case of the ion-milled specimens, there is additional diffuse scattering from amorphous surface layers produced by the milling.

4. Interpretation of the results

The GIXRD spectra were interpreted using the JCPDS database. The reflection peaks shown in spectrum 2a are mainly due to the wurtzite

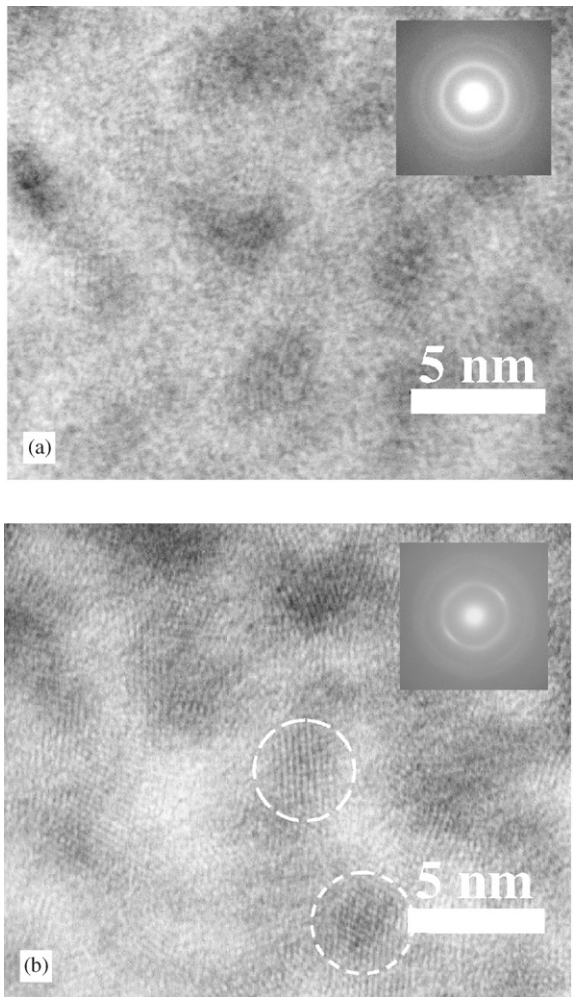

Fig. 5. HRTEM micrographs of (a) type 2 and (b) intermediate type samples prepared by ion milling of thick films.

(hexagonal) CdS structure, while spectrum 2c appears to indicate that two phases may be present, although a significant contribution from the Al_2O_3 may be included. In order to determine the exact position of the CdS and Al_2O_3 reflection peaks, a deconvolution procedure of the spectra was undertaken, after background subtraction. In order to deconvolute the overlapping peaks, several pseudo-Voigt functions, one for each crystallographic diffraction orientation of the hexagonal CdS and Al_2O_3 structures, were used. The fitting of type 1 samples (Fig. 6a) shows a

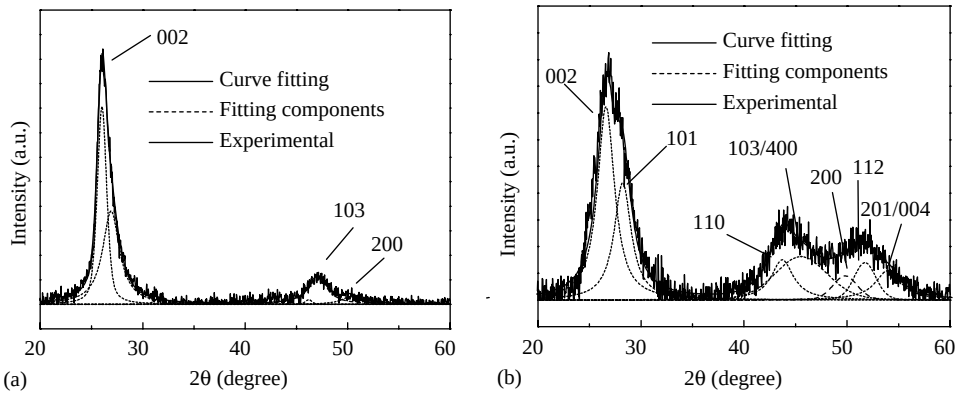

Fig. 6. Experimental diffractograms and their curve fitting. Different pseudo-Voigt functions were taken into account in the fitting procedure: (a) type 1 sample, (b) type 2 sample.

Table 2
Crystallographic data from JCPDS files and experiment

(hkl)	JCPDS database		TYPE 1 samples			
	CdS	Al_2O_3	A	B	C	D
	24.808					
(0 0 2)	26.507		26.36/26.97	26.24/27.06	26.09/26.57	26.26/26.89
	28.183					28.10
		32.80				
	43.682					
		45.64				
(1 0 3)	47.840		47.60	47.51	47.09	47.58
	50.883		49.96			
	51.825					
	52.798					
	54.586					
I^{002}/I^{103}	1.82		5.64	3.92	7.33	3.65

doublet centred around $2\theta = 26.2^\circ/26.9^\circ$, corresponding to a splitting of the (0 0 2) reflection of CdS (whose meaning will be discussed later) and another peak at $2\theta \approx 47.3^\circ$. Moreover, very small contributions can also be seen at $2\theta \approx 31^\circ$, 46° and 50°. The characteristic full-width at half-maximum (FWHM) of the global 002 peak is about 1.3° while the peak centred at 47.3° has a higher FWHM of about 3.0°. Importantly, the mean size of the crystals could be estimated from the GIXRD results because the average size of crystallites can be related to the broadening of the reflection peaks according to the Scherrer equation [13]. Values of about 7.5 and 4 nm were thus obtained for the [0 0 2] and the [1 0 3] directions, respectively. This size difference indicates a higher growth rate of the crystallites along the [0 0 2] direction yielding the development of non-spherical crystallites. Also, by comparing the intensity ratio I^{002}/I^{103} between the experimental data and the JCPDS tabulated values (Table 2), it can be concluded that films with a preferred orientation are developed for the experimental conditions leading to type 1 samples.

Fig. 6b shows the result of the fitting of one diffractogram recorded for a type 2 sample and its

individual components. Several reflection lines such as 002, 101, 110, 103, 200, 112, 201 and 004 for CdS and 400 for alumina were taken into account in the fitting procedure. The FWHM varies in the 2θ range from $\sim 2.0^\circ$ at 26° to $\sim 3.0^\circ$ at 50°, i.e. as the reciprocal of $\cos\theta$, indicating the presence of almost rounded crystallites. Applying the Scherrer equation to all the diffracted lines displayed by each sample, a nanocrystallite mean size between 3.7 and 4.4 nm was calculated.

Turning to the GIXRD spectra of Fig. 3a, the fitting procedure applied to the diffractograms of the annealed samples indicates that one peak at $2\theta \sim 26^\circ$ is sufficient to fit the low 2θ region. This peak corresponds to the lower angle peak of the (0 0 2) doublet observed in the as-deposited samples, which increases in intensity whereas the higher angle doublet peak disappears, even at the lowest annealing time of 2 h. As can be observed from the spectra of the annealed samples as compared to the as-deposited one, the 002-diffraction line is shifted from its initial position as the annealing time is increased. Simultaneously, the FWHM of the peak decreases from $\sim 1.3^\circ$, in the as-deposited sample, to $\sim 0.9^\circ$. Analogous trends are also observed for the (1 0 3) peak at $\sim 47^\circ$, the FWHM being reduced from $\sim 3.0^\circ$ to $\sim 2.0^\circ$ in this case. The reduction in the 002-FWHM indicates an increase in the dimension of the crystallites from 7.5 to 8.9 nm.

For type 2 samples, although the annealing procedure was similar to the one followed for type 1 samples, it does not lead to any significant modification of the material structure as can be observed from the analysis of Fig. 3b. As can be seen, the peaks do not change in position when the sample was annealed, maintaining their standard values, although the grain size slightly increased with annealing time, from 3.7 to 4.2 nm. The fitting results discussed above for both types of samples are compared in Fig. 7, where we have plotted the evolution of grain size and peak position with annealing time. The effect of annealing is significant for type 1 samples, leading to an average size increase of about 1.4 nm.

The HRTEM images confirm the above results showing that CdS nanocrystals are readily formed at room temperature. Furthermore, these images leave no doubt that the nanocrystals are formed during the early stages of the deposition process, as can be observed in Fig. 4, which displays the image of a very thin film (~ 16 nm) deposited over the carbon film on a copper grid. From this figure it can also be seen that some of the nanocrystals

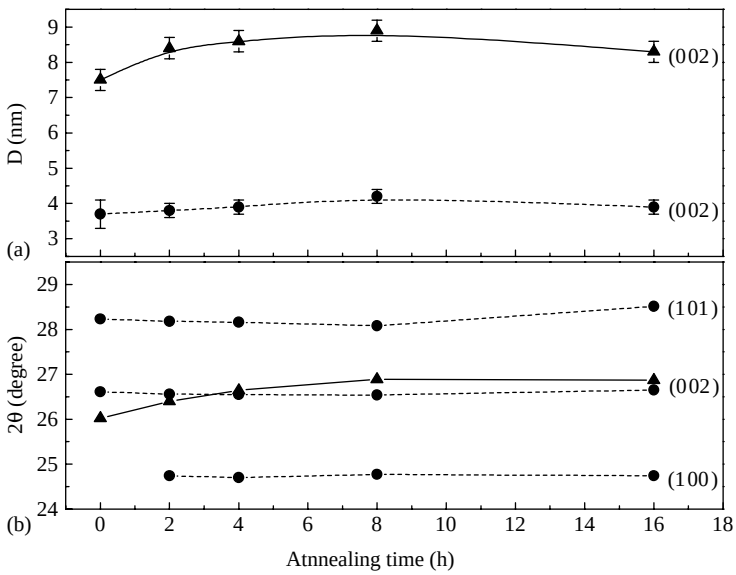

Fig. 7. Variation of (a) grain size and (b) peak position with annealing time for type 1 (triangles) and type 2 samples (circles).

are elongated and differently oriented. Most of them exhibit only one family of planes whose inter-spacing distance is characteristic of {0 0 2} planes in the wurtzite structure or of {1 1 1} planes in the zincblende (cubic) structure. Particles marked with arrows in Fig. 4 have a length of ~ 7.5 nm, which agrees well with particle size inferred from XRD for type 1 samples. Furthermore, a few particles display two families of planes that allow us to identify the crystallographic structure. For instance, numerical Fourier transform performed on particle A in Fig. 4 yield an interplanar spacing of ~ 0.33 nm and an angle between the diffraction directions of 70°, which corresponds to diffraction by (1 1 1) planes in CdS with the zincblende structure.

Fig. 5 was obtained from two films prepared by the classical method and then thinned, as described in the experimental section. Following the classification adopted for the XRD, these samples are of type 2 (Fig. 5a) and of intermediate type (Fig. 5b). In both cases, a greater number of crystals are present than are seen in Fig. 4, which make difficult their individual study (like shape, size and orientation). However, it is possible to estimate the mean size of the particles to be around 3 nm just by using the grey colour contrast in the micrographs. From the ED patterns there is an obvious difference between the two samples. While in Fig. 5a, the ED rings can be assigned to reflections originating from randomly oriented crystals of small size, the ED of Fig. 5b shows diffraction rings that can be attributed to a sample exhibiting a certain degree of texture. Unfortunately, those samples that are strongly textured as observed from XRD are too brittle and could not withstand the required preparation for TEM analysis.

5. Discussion

The cubic structure of zincblende (B) and the hexagonal structure of wurtzite (W) are the two types of atomic arrangements adopted by tetrahedrally coordinated semiconductors of the II–VI groups. Bulk cadmium sulphide compounds crystallise in the W-structure. As far as nanocrystals are concerned, it has been shown [9] that depending on the average size of the crystallites either the (B) or (W) structure may be expected. Particles between 3 and 4 nm in diameter, crystallise preferentially in the cubic structure of the zincblende ($a = 0.5818$ nm), which is a metastable phase favoured by the nucleation kinetics. For larger particles (average size larger than 6 nm), the stable structure of wurtzite ($a, b = 0.4136$ nm and $c = 0.6713$ nm) is the usually encountered. In between, nanocrystals form with intermediate structures, consisting of B-type structure with stacking faults and twins, or a two-phase structure composed of B- and W-type domains sharing close packed planes [9].

The results obtained in the present work show that in the case of co-sputtering of CdS and alumina, the growth of the CdS nanocrystals embedded in the alumina matrix is always accompanied by the development of an hexagonal structure, although the cubic structure may also be present depending on the deposition conditions. As we have seen, at low argon pressure and RF-power values, the (0 0 2) peak is very prominent and in the high 2θ range values, above 40°, only the (1 0 3) reflection from the hexagonal phase can be observed, allowing us to assign a textured hexagonal structure to type 1 thin films. Textured samples were also observed by TEM in the case of samples grown with intermediate process parameters (Fig. 5b). Conversely, for high argon pressure or RF-power, samples display the complete pattern of the hexagonal phase, which indicates that the CdS nanocrystals are randomly oriented. It can also be assumed that the nanocrystals are spheroids, because the crystallite sizes that were calculated for every single peak closely follow the $(\cos\theta)^{-1}$ law. However, because the main reflections for the zincblende structure overlap some of those for the wurtzite structure, it is also possible that the diffraction patterns in Figs. 2b and c result from the co-existence of both phases in the deposited material. This is supported by previous work [9] where the B-type structure was associated with very small crystals. Other evidence for possible co-existence of cubic and hexagonal phases in the grown films is given by the TEM results obtained on a very thin film of the

Table 3
Strain parameter, ε, for type 1 samples

Type 1 sample	$\Delta(2\theta)_{0\,0\,2} = 2\theta_{exp} - 2\theta_{tab}$ ($2\theta_{tab} = 26.507^\circ$)	$\varepsilon = -\Delta\theta/\tan\theta$
As-deposited	−0.419	1.5×10^{-2}
Annealed (2 h)	−0.132	4.9×10^{-3}
Annealed (4 h)	0.143	-5.3×10^{-3}
Annealed (8 h)	0.335	-1.2×10^{-2}
Annealed (16 h)	0.326	-1.2×10^{-2}

type 1 (Fig. 4), where a detailed analysis showed the presence of nanocrystals with both hexagonal and cubic symmetries. Our interpretation is that during the early stages of film growth, nanocrystals develop mainly with zincblende structure. As deposition proceeds, the number of nanocrystals exhibiting the wurtzite structure increases, probably due to an increase of the surface temperature caused by the increasing bombardment of the growing film by the particles in the RF-plasma.

In addition, the (0 0 2) peak position in type 1 diffraction patterns is clearly below the reference value of 26.507° given by JCPDS card no. 41-1049. As mentioned in Section 4, this peak is effectively a doublet, because its fitting is best achieved with two pseudo-Voigt functions centred on slightly different angles. When type 1 samples were annealed, the global $2\theta_{0\,0\,2}$ moves towards higher angles, as is shown in Figs. 6a and 7b, because the sub-peak at the lower angle shrinks away. If we associate this angular shift with a strain parameter, ε, derived from equation $\Delta\theta = -\varepsilon * \tan\theta$, we can build Table 3. The results indicate that increasing the annealing time from 2 to 16 h yields a variation in strain parameter. For short annealing times (up to $\approx$2 h), the CdS nanocrystals are under the influence of tensile stress; as annealing time increases, stresses become compressive. A better understanding of these structural changes can be achieved if the hexagonal lattice parameters, a and c, are calculated. This reveals for type 2 samples that the structural parameters remain constant with annealing time ($a = 0.414$ and $c = 0.670$ nm) indicating that the growth of the nanocrystals proceeds free of stresses. In comparison, an increase in the annealing time for type 1 films leads to a decrease in c from $c = 0.681$ to 0.665 nm, which is lower than the tabulated value. Parameter a remains almost constant ($a \approx 0.413$ nm) when compared with the standard value.

The overall results presented above can be understood in the framework of correlations between the internal structures of the film components (matrix and semiconductor) during the deposition process, mainly through the influence of the PVD deposition parameters (deposition rate, argon pressure and RF-power). Indeed, we can conjecture about the links between the deposition conditions and the microstructures of the samples, and hence with their macroscopic properties. The conditions for type 1 samples are low argon pressure and RF-power well below 200 W, so that the number of atoms that strike the film surface during growth is high, leading to high deposition rates. Low-porosity films are nucleated on the substrate from sputtered atoms that strike with high kinetic energies and have high mobilities, but only on the free growth surface [12]. The microstructure of such a film is very quickly established and then frozen. Equilibration of the randomly oriented CdS nanocrystallites is not possible, because of lack of bulk diffusion. This explains the strain observed in the type 1 films, which have a corresponding tendency to delaminate from their substrates.

Lower deposition rates correspond to high argon pressure (equal to 9×10^{-3} mbar) and RF-power approaching 200 W and these conditions lead to type 2 films. The sputtered atoms strike the free surface with low energy and there are longer times between successive arrivals because of the high collision rates of the particles inside the plasma. Such factors lead to microstructures of lower density than those of type 1 films [12]. In these more defective and slower-growing films some diffusion is possible (via internal pore surfaces and probably also in the bulk), so that CdS nanocrystals favour the easy growth directions and tend to equilibrate. One might expect this to be manifest by the formation of faceted rather than spherically shaped crystals, so we

conclude that the nanocrystals are too small for visible faces to develop. The resulting microstructures produce stress-free films.

6. Conclusions

Thin films consisting of CdS nanocrystals embedded in Al_2O_3 matrix have been successfully produced by magnetron RF-sputtering at room temperature.

GIXRD was used for phase and texture characterisation. Investigation by HRTEM revealed the nanocrystalline nature of the CdS particles. It also showed that they tend to crystallise in the cubic phase (zincblende structure) during the early stages of film growth, but the growth process leads to the evolution of a mainly hexagonal phase.

Depending on the experimental parameters, two types of crystals could be obtained. Type 1 samples present a preferred growth along the *c*-axis, which aligns approximately along the normal to the plane of the film and is therefore roughly parallel to the direction of the incident particle flux. In type 2 samples, there is no evidence of a preferred growth orientation. Type 1 crystals have a non-spherical shape with an average size of about 7.5 nm in the (0 0 2) direction and 4.0 nm in the (1 0 3) one. Type 2 crystals have a near-spherical shape with a mean diameter value between 3.7 and 4.4 nm. It has also been observed that with a proper choice of the experimental parameters, films with intermediate microstructures can be grown.

GIXRD studies indicated that as-grown films are under tensile stress which evolves to compressive stress when the films are annealed. The as-deposited type 2 samples did not show the presence of stresses in the material, and no changes were observed from XRD patterns after annealing the samples.

Acknowledgements

This work has been partially funded through the projects FCT-POCTI/FIS/10128/98, BC/CRUP—Treaty of Windsor Program No. B 23/02 and French Embassy/ICCTI Research Program No. 321 B1. The authors wish to thank the electron microscopy staff for providing us with the possibility of using the Philips CM20 TEM (Châtillon-Montrouge, Paris, France) and M.J. Reece for access to the JEOL 2010 microscope (Queen Mary College, London, England).

References

[1] P.D. Persans, H. Yukselici, L.B. Lurio, J. Pant, M. Stapleton, T.M. Hayes, J. Non-Cryst. Solids 203 (1996) 192.
[2] S. Gorer, G. Hodes, Y. Sorek, R. Reisfeld, Mater. Lett. 31 (1997) 209.
[3] P. Facci, M.P. Fontana, Solid State Commun. 108 (1998) 5.
[4] M.V. Artemyev, A.I. Bibik, L.I. Gurinovich, S.V. Gaponenko, H. Jaschinski, U. Woggon, Phys. Stat. Sol. B 224 (2001) 393.
[5] A.G. Rolo, O. Conde, M.J.M. Gomes, Thin Solid Films 318 (1998) 108.
[6] C.W. White, J.D. Budai, S.P. Withrow, J.G. Zhu, E. Sonder, R.A. Zuhr, A. Meldrum, D.M. Hembree Jr., D.O. Henderson, S. Prawer, Nucl. Instrum. Methods B 141 (1998) 228.
[7] A. Balandin, K.L. Wang, N. Kouklin, S. Bandyopadhyay, Appl. Phys. Lett. 76 (2000) 137.
[8] A. Ekimov, J. Lumin. 70 (1996) 1.
[9] C. Ricolleau, L. Audinet, M. Gandais, T. Gacoin, Thin Solid Films 336 (1998) 213.
[10] A. Meldrum, E. Sonder, R.A. Zuhr, I.M. Anderson, J.D. Budai, C.W. White, L.A. Boatner, D.O. Henderson, J. Mater. Res. 14 (1999) 4489.
[11] R. Swanepoel, J. Phys. E 16 (1983) 1214.
[12] Aimé Richardt, Anne-Marie Durand, Les Interactions Ions Énergétiques-Solides, IN FINE, Paris, 1997 (Chapters 8 and 11).
[13] B.D. Cullity, Elements of X-ray Diffraction, 2nd Edition, Addison-Wesley, Reading, MA, 1978, p. 102.